Science of the Total Environment 812 (2022) 152447

Contents lists available at ScienceDirect

Science of the Total Environment

journal homepage: www.elsevier.com/locate/scitotenv

Reconciling the bottom-up methodology and ground measurement constraints to improve the city-scale NMVOCs emission inventory: A case study of Nanjing, China

Rongrong Wu [a], Yu Zhao [a,b,*], Sijia Xia [c], Wei Hu [d], Fangjian Xie [e], Yan Zhang [f], Jinjin Sun [d], Huan Yu [g], Junlin An [h], Yutong Wang [a]

[a] State Key Laboratory of Pollution Control & Resource Reuse and School of the Environment, Nanjing University, 163 Xianlin Ave., Nanjing, Jiangsu 210023, China
[b] Collaborative Innovation Center of Atmospheric Environment and Equipment Technology, CICAEET, Nanjing, Jiangsu 210044, China
[c] Jiangsu Key Laboratory of Environmental Engineering, Jiangsu Provincial Academy of Environmental Sciences, Nanjing, Jiangsu 210036, China
[d] Jiangsu Key Laboratory of Atmospheric Environment Monitoring and Pollution Control, School of Environmental Science and Engineering, Nanjing University of Information Science and Technology, Nanjing 210044, China
[e] Nanjing Municipal Academy of Ecology and Environment Protection Science, Nanjing, Jiangsu 210093, China
[f] Jiangsu Environmental Engineering and Technology Co., Ltd, Jiangsu Environmental Protection Group Co., Nanjing, Jiangsu 210019, China
[g] School of Environmental Studies, China University of Geosciences, Wuhan, Hubei 430074, China
[h] Collaborative Innovation Center on Forecast and Evaluation of Meteorological Disasters, Key Laboratory for Aerosol-Cloud-Precipitation of China Meteorological Administration, Nanjing University of Information Science and Technology, Nanjing, Jiangsu 210044, China

HIGHLIGHTS

- A NMVOCs emission inventory was developed with best available source information.
- 105 NMVOCs species were measured for one year in five different functional zones.
- The constrained emission from observation was 81% larger than the bottom-up estimate.
- Model performance of O_3 simulation was improved with constrained NMVOCs emissions.
- Surface coating, on-road vehicles and oil refinery were the main sources to reduce O_3.

GRAPHICAL ABSTRACT

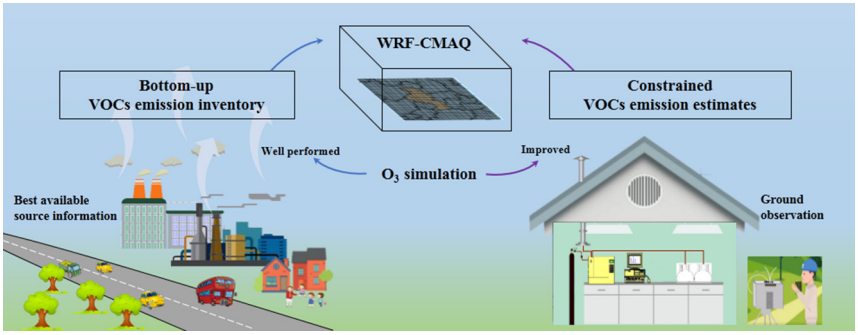

ARTICLE INFO

Article history:
Received 19 October 2021
Received in revised form 7 December 2021
Accepted 12 December 2021
Available online 21 December 2021

Editor: Chennai Guest Editor

Keywords:
NMVOCs
Emission inventory
Constraint

ABSTRACT

Reliable emission estimate of non-methane volatile organic compounds (NMVOCs) is important for understanding the atmospheric chemistry and formulating control policy of ozone (O_3). In this study, a speciated emission inventory of anthropogenic NMVOCs was developed with the refined "bottom-up" methodology and best available information of individual sources for Nanjing in 2017. The total NMVOCs emissions were calculated at 163.2 Gg. It was broken down into the emissions of over 500 individual species and aromatics took the largest fraction (33.3% of the total emissions). Meanwhile, 105 compounds were measured at 5 sites representing different functional zones of Nanjing for one year. The annual mean concentration of totally 105 species varied from 48.5 ppbv to 63.7 ppbv, and alkanes was the most abundant group with its mass fractions ranging 37.2–40.1% at different sites. Constrained by the emission ratios of individual species versus carbon monoxide (CO) based on ground measurement, the total emissions of 105 species (NMVOCs-105) was estimated at 195.6 Gg, 81.1% larger than the bottom-up estimate of NMVOCs-105 (108.0 Gg). The constrained emissions indicated an overestimation of aromatics and underestimation of OVOCs and halocarbons

* Corresponding author at: State Key Laboratory of Pollution Control & Resource Reuse and School of the Environment, Nanjing University, 163 Xianlin Ave., Nanjing, Jiangsu 210023, China.
E-mail address: yuzhao@nju.edu.cn (Y. Zhao).

http://dx.doi.org/10.1016/j.scitotenv.2021.152447

CMAQ
Ozone formation potential

in the bottom-up emission inventory because of the uncertainties in source profiles. O_3 simulation with Community Multi-scale Air Quality (CMAQ) model was conducted for January, April, July and October in 2017 to evaluate the bottom-up and constrained emission estimates. The mean normal bias (MNB) and mean normal error (MNE) values were generally within the criteria (MNB $\leq \pm 15\%$ and MNE $\leq 30\%$) for both inventories. The model performance was improved when the constrained estimates were applied, indicating the benefit of ground observation constraints on NMVOCs emission estimation and O_3 simulation. Based on the O_3 formation potential (OFP), 12 key NMVOCs species mainly from surface coating, on-road vehicles and oil exploitation and refinery were identified as the priority compounds for O_3 reduction.

1. Introduction

Non-methane volatile organic compounds (NMVOCs) play an important role on the ground-level ozone (O_3) formation (Toro et al., 2006). In the presence of sunlight, NMVOCs can react with hydroxyl radicals (•OH) and oxides of nitrogen (NO_X) to form O_3 through a series of photochemical reaction (Atkinson, 2000). Along with gradually reduced ambient particulate matter (PM) levels, O_3 pollution has become an increasingly severe problem in China (Liang et al., 2021; Qiao et al., 2019), motivating better understanding and control of NMVOCs emissions. NMVOCs include various kinds of chemical substances such as non-methane hydrocarbons (NMHCs, including alkanes, alkenes, alkynes and aromatics), oxygenated VOCs (OVOCs, including aldehyde, ketone, ester, ether, alcohol and organic acid), and halogenated hydrocarbons (halocarbons). The major sources of NMVOCs are the natural processes (i.e., vegetation emissions, volcanic eruption and forest fire) at the global scale (Guenther et al., 2006), while they are mainly emitted from anthropogenic activities in urbanized areas, such as vehicular exhausts, solvent usage, industrial chemical and petrochemical processes (Janssens-Maenhout et al., 2015). Compared to other anthropogenic air pollutants like SO_2 and NO_X, complex sources and big diversity of emission levels were found for individual NMVOCs species. The magnitude, spatiotemporal distribution, and source contribution of anthropogenic NMVOCs emissions have become increasingly important for atmospheric chemistry studies and air quality improvement, particularly in fast urbanization countries like China (Guo et al., 2017).

The "bottom-up" method has been widely used to evaluate NMVOCs emissions. It calculates the emissions by multiplying the activity levels and corresponding emission factors by source category. The national and regional emission inventories in China have been developed and improved gradually in recent years, with plant-level activity data of certain emission sources and domestic measurement results of emission factors incorporated (An et al., 2021; Li et al., 2019c; Zhong et al., 2018; Wu and Xie, 2017; Zhao et al., 2017; Ou et al., 2015). As cities are the fundamental administration for air quality improvement in China, there is a further strong need of reliable city-level emission inventories for the development of air pollution control programs and supervision of air pollutant emissions. Unfortunately, very few city-scale NMVOCs emission inventories were available and the uncertainty remained large, attributed to the relatively coarse statistics or insufficient investigations on individual emission sources. Most researches had to rely on provincial-level statistical data and national uniform emission factors, and then downscaled the calculated emissions to the city level. Besides, motivated by the increased O_3 pollution in urban China, various measures have been implemented to control NMVOCs in recent years, such as the improving standards regarding NMVOCs emissions for surface coating industries, the implementation of Leak Detection and Repair (LDAR) program for petrochemical industries and the promotion of new green energy vehicles for transportation sources (Zhao et al., 2020). The benefit of those measures on emission abatement has not been well included in the emission inventory development, as the emission control information was not regularly reported. As essential input data for chemical transport model (CTM), existing NMVOCs emission inventories were expected to result in large bias of air pollution simulation, especially for O_3 simulation at small spatial scales (Karl et al., 2009; Warneke et al., 2007). It further introduced uncertainty in evaluating O_3 pollution and formulating O_3 control policy. Besides the total emission magnitude and spatial allocation, chemical speciation is another important factor influencing modeling performance due to the varied reactivities of different NMVOCs species (Carter, 2010). The uncertainties of NMVOCs source profiles were still large resulting from the insufficient coverage of measured categories and the limited amounts of measured species.

Studies have been conducted to evaluate and verify the NMVOCs emission inventories based on satellite retrievals or ground measurements. Given its broad spatial coverage but coarse temporal resolution, satellite observation was often applied at the global or national scale to evaluate the spatial pattern of the bottom-up emission inventories (Liu et al., 2012; Fu et al., 2007). In contrast, ground observation was usually used at the regional or city scale limited by its spatial coverage. Previous studies evaluated anthropogenic emissions of individual NMVOCs species in Beijing (Li et al., 2019a; Wang et al., 2014), Chengdu (Simayi et al., 2020), and the Pearl River Delta (PRD) region (Shao et al., 2011), with a tracer ratio method based on ground observation. In the Yangtze River Delta (YRD) region, Wang et al. (2020a) combined ground observation with regional air quality modeling in Shanghai and found that current bottom-up estimates of NMVOCs emissions were highly biased. The measurements in most of those studies were conducted at a single site or in a specific season, and thus not sufficient for evaluating the spatial and temporal distribution of NMVOCs. Megacities consist of different functional zones, such as industrial parks, residential areas, and transportation hubs, where the emission sources differ from each other (Hu et al., 2018). Observations with greater spatial and temporal coverage are needed to better constrain NMVOCs emissions.

Located in the western YRD region, Nanjing is a highly urbanized and industrialized city. The main industries in Nanjing, including petrochemical industries, electronics industries, automobile coating and iron & steel production, are the major sources of NMVOCs. Traffic is also an important source due to the rapid growth in vehicle population in the city (NJNBS, 2018). In recent years, O_3 pollution became a significant factor affecting the air quality of Nanjing (Wang et al., 2020b). The photochemical O_3 formation regime was identified as VOC-limited in the urban areas of Nanjing (Zhao et al., 2020), thus limiting NMVOCs emissions and concentrations should be a priority for reducing O_3 pollution. In this study, we aim to improve the NMVOCs emission inventory and the model performance of O_3 simulation at the city scale, combining the detailed information of local emission sources, ground measurements and CTM. A bottom-up emission inventory of anthropogenic NMVOCs was developed for Nanjing in 2017. The ambient levels of NMVOCs were measured at five observation sites located in different city functional zones to evaluate the spatiotemporal pattern of NMVOCs. The emission ratios (ERs) calculated based on the observation data were then applied to constrain the NMVOCs emissions. The bottom-up and the constrained emission estimates were further evaluated and compared using CTM. Species with large contribution to O_3 formation potential (OFP) were identified and NMVOCs emission control strategies for Nanjing were recommended. The outcome of this study could serve as a more scientific basis for NMVOCs emission control and O_3 pollution alleviation for developed cities.

2. Methods

2.1. Development of the bottom-up emission inventory

2.1.1. Emission estimation

A four-level structure was used to classify the anthropogenic NMVOCs sources, as summarized in Table S1 in the Supplement. Level 1 included

seven categories, i.e., fossil fuel combustion, industrial processes, solvent usage, transportation, oil distribution, biomass burning and others. Level 1 sources were then further divided into Levels 2–4 according to the different processes, raw materials, products, or fuel types. Totally 113 sources were comprised in Level 4. In this work, detailed information on NMVOCs emission sources were collected and complied for Nanjing based on various databases. Those databases contained the Second National Census on Pollution Sources (SNCPS) in China, the official environmental statistics, and a new local survey dataset of main NMVOCs industries developed by Jiangsu Provincial Academy of Environmental Science (JPAES). SNCPS and environmental statistics provided basic information at plant level, including geographic location, types and amounts of raw materials and products, fuel quality and consumption, and combustion/manufacturing technology. Besides, more detailed information at production procedure level were collected in local survey dataset, such as operation time, collection equipment of flue gas, flow rate and NMVOCs concentration in flue gas, the implementation of LDAR, NMVOCs content in solvent, and collection and removal efficiencies. Individual enterprises were required by local government to submit those data, which were further examined and refined through cross check, on-site investigation and measurements.

NMVOCs emissions from fossil fuel combustion, industrial processes and industrial solvent usage (including surface coating and printing) were estimated at production procedure (Eq. (1)) or plant level (Eq. (2)) according to the obtained information for each enterprise:

$$\mathrm{E_i} = \sum_{k=1}^{n}\sum_{p=1}^{m} E_{\mathrm{p},k} \times \left(1-\eta_{p,k}\right) \tag{1}$$

$$\mathrm{E_i} = \sum_{k=1}^{n} EF_{\mathrm{k}} \times A_{\mathrm{k}} \times \left(1-\eta_{k}\right) \tag{2}$$

where E_i stands for the total emissions of source category i, $E_{p,k}$ stands for the emission from production procedure p of enterprise k, $\eta_{p,k}$ is the removal efficiency of end-of-pipe treatment facility in corresponding production procedure p of enterprise k, EF_k, A_k and η_k represent the uncontrolled emission factor, activity data and removal efficiency of enterprise k respectively, and m and n represent for the number of production procedures in enterprise k and the number of enterprises related to source category i respectively.

Details on procedure-level methods could be found in Zhang et al. (2021) and Guidelines for NMVOCs Pollution Source Investigation in Petrochemical Industry (MEP, 2015b). Briefly, the production procedures of each enterprise were divided into six processes, including manufacturing lines, equipment leaks, storage tanks, loading operations, wastewater collection and treatment system, and circulating water systems. Best available method was applied for each procedure with priority. For example, measurement-based method was chosen firstly if the monitoring results were available, such as flow rate, NMVOCs concentrations in flue gas, the capture efficiency for fugitive emissions, and emission rate from LDAR program. The mass balance method was the second choice if NMVOCs contents in raw materials and outputs were accessible. The third was the empirical formula method, requiring physical and chemical parameters of materials, and the forms and quantities of material loading/storing. Default emission factors for each procedure were applied if above information could not be obtained (MEP, 2015b; SMBEE, 2017).

The activity data at procedure level were provided for 1265 enterprises in the local survey dataset (250 plastic and rubber plants, 164 raw chemicals manufacturing plants, 137 furniture manufacturing plants and 714 other industrial factories). The proportions of different methods are summarized by procedure in Table S2 in the Supplement. The measurement-based method accounted for 53% of manufacturing lines and 78% of equipment leaks. Additionally, NMVOCs emissions of 4858 enterprises were calculated at plant level, including 24 power plants, 383 heating/industrial boilers sources, 1424 industrial solvent usage sources and 3434 industrial processes sources. The activity data including fuel consumption, solvent usage, and industrial production output were obtained from SNCPS, environmental statistics, and the local survey dataset. As summarized in Table S1 in the Supplement, the uncontrolled emission factors came mainly from the compilation guidelines for the NMVOCs emission inventories (MEP, 2014), the guidebook of emission inventory development for Chinese cities (He, 2018) and recent published results. In particular, NMVOCs contents of solvents from local survey dataset were applied as emission factors for industrial solvent usage sources.

Table S3 in the Supplement summarizes the penetrations and removal efficiencies of end-of-pipe treatment facilities, submitted by 1853 enterprises in the local survey dataset. Approximately 50% of enterprises were equipped with treatment facility, and adsorption made a significant proportion (30.2%). Larger removal efficiencies were found for regenerative thermal oxidizer and direct burning, with a range at 72.3–94.7% and 28.6–99.1%, respectively. The removal efficiencies of adsorption and photocatalytic oxidation had a wide range, from 1.4% to 99.7% and from 9.9%–97% respectively, indicating the difference of operation and maintenance among various enterprises. For absorption, spray and other single treatment, the removal efficiencies were generally lower than 50%. For industrial plants without monitored removal efficiencies, the values of different treatment facilities were assumed from 15% to 85%, as shown in Table S3 in the Supplement.

NMVOCs emissions of non-industrial solvent usage, transportation, oil distribution, biomass burning and others were estimated as the product of emission factors and activity data by source category. Activity data of oil distribution were obtained from local survey dataset and biomass burning from SNCPS. Other activity data such as populations, building areas, fuel consumption, and vehicle population were obtained from statistical yearbook (NJNBS, 2018). Emission factors were mainly from the guidebook of emission inventory development for Chinese cities (He, 2018), as listed in Table S1 in the Supplement.

The emissions of individual NMVOCs species were calculated as follows:

$$E_{\mathrm{i,j}} = E_i \times P_{i,j} \tag{3}$$

where $E_{i,j}$ is the emissions of species j from source category i, E_i is the total NMVOCs emissions from source category i, and P_{ij} is the mass fraction of species j in emission source category i (i.e., the source profile). The source profiles used in this study were obtained from Wu and Xie (2017) and Zhao et al. (2017).

2.1.2. Spatial and temporal allocation

The NMVOCs emissions were spatially allocated at a horizontal resolution of 3 km × 3 km according to the real locations of point sources and surrogate indexes of others. Accurate geographical locations of totally 6123 point sources (Fig. 1) were obtained and their emissions were allocated into corresponding grid cells. The distribution of gross domestic product (GDP) with high resolution at 1 km was applied to allocate the emissions from oil distribution, waste disposal, construction machinery and other industrial related sources. The distribution of population was applied to allocate the emissions from residential and commercial sources. The emissions from on-road transportation were allocated based on the road net weighted by traffic flow, and those from ships based on the area of river. The emissions from pesticide usage, biomass burning and agricultural machinery were allocated based on the density of cultivation area. The spatial distribution of land use types, population, and GDP was obtained from the Data Center for Resources and Environmental Sciences of the Chinese Academy of Sciences (www.resdc.cn/). The temporal allocation was performed following monthly profiles in our previous studies (Zhao et al., 2017; Zhou et al., 2017), as shown in Table S4 in the Supplement.

2.2. Constrained species-specific NMVOCs emissions with ground measurement

2.2.1. Observation sites

NMVOCs measurements were conducted at five sites representing different types of functional zones in Nanjing, as shown in Fig. 1. PAES (32.05°N, 118.74°E) is located on the roof of an office building of Jiangsu

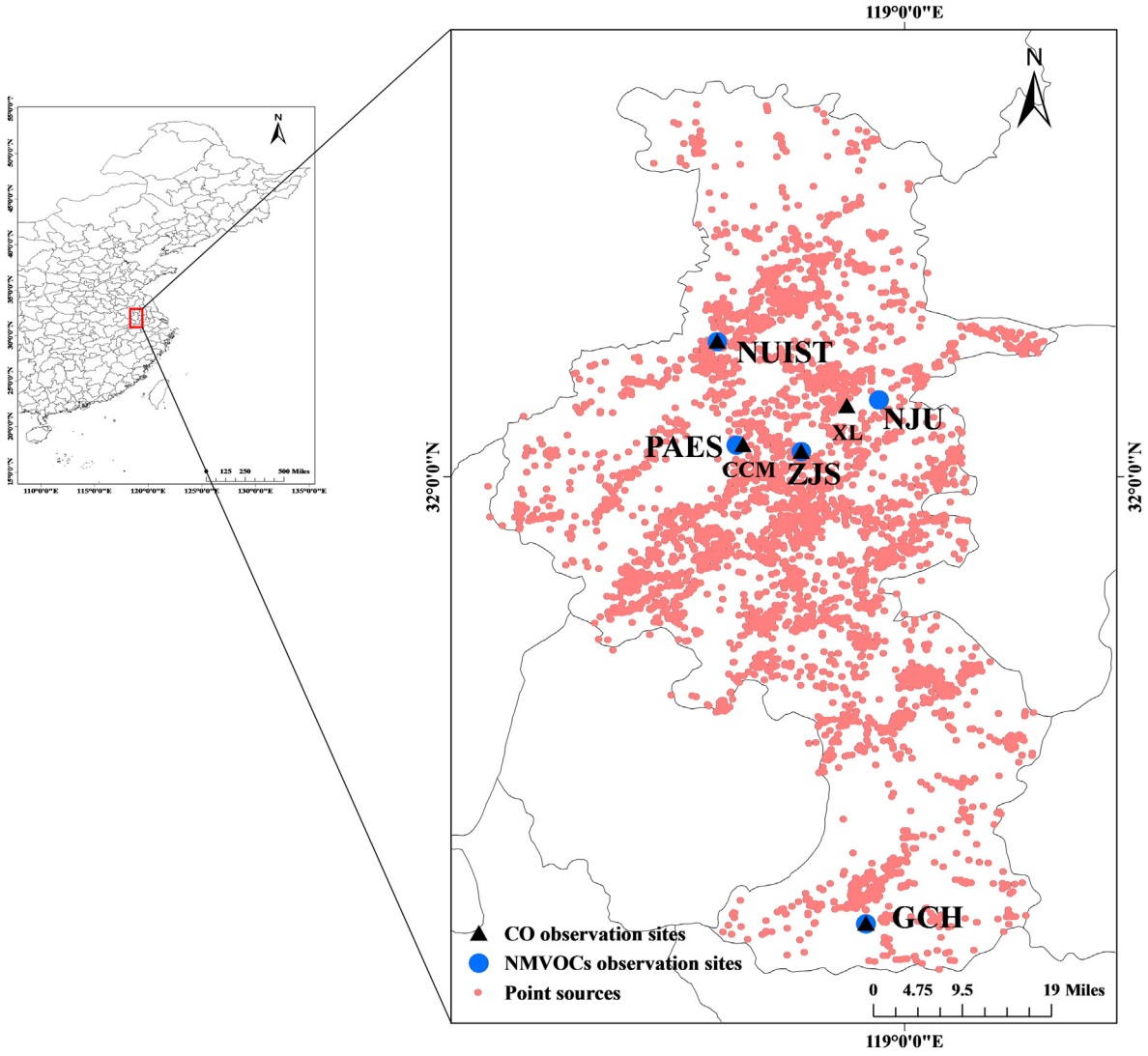

Fig. 1. The locations of point sources and observation sites.

Provincial Academy of Environmental Science. It is a typical urban site, surrounded by abundant traffic and residential and commercial buildings (Zhao et al., 2020; Chen et al., 2017). NJU (32.12°N, 118.96°E) is a suburban site, located in the Xianlin Campus of Nanjing University, approximately 20 km from downtown (Wu et al., 2020; Chen et al., 2017). NUIST (32.21°N, 118.71°E) is located in the Nanjing University of Information Science & Technology campus. It is a polluted industrial site due to the influence from Nanjing Chemical Industry Park (NCIP), iron & steel plants, and power plants nearby (Chen et al., 2017; An et al., 2014). ZJS (32.04° N, 118.84° E) is located in the urban forest park Zijin Mountain, with a forest area of 22 km^2. It is also a tourist attraction thus can be influenced by NMVOCs from touring vehicles. GCH (31.31°N, 118.94°E) is located by the Gucheng Lake, surrounded by water body and farmlands with tiny anthropogenic emissions.

Carbon monoxide (CO) was observed as a tracer at the sites except PAES and NJU, due to the technical problems with the instruments at the two sites during the sampling period. Instead, the data reported at two state-operating air quality observation sites, CCM and XL (Fig. 1), were used to represent the atmospheric conditions around PAES and NJU, respectively (Wu et al., 2020; Chen et al., 2017).

2.2.2. Sampling and chemical analysis

The online observations of ambient NMHCs at NJU were conducted at an interval of 1 h from May 2017 to April 2018. A more detailed description of this system has been provided in previous study (Wu et al., 2020). The offline measurements were conducted using silica stainless steel canisters from May 2017 to May 2018. Ambient samples were collected five days every month at PAES, NUIST and ZJS, two days every month at NJU and five days every season at GCH. The temporal variation of air pollution was expected to be less influenced by that of local emission sources at the rural site GCH, thus the sampling frequency was decreased. Non-rainy days with low wind speed were usually chosen as sampling days and the sampling times were around 9:00 am and 2:00 pm, respectively. Totally 408 air samples were obtained in this study.

Prior to sampling, all canisters were cleaned at least five times by repeatedly filling and evacuating ultra-pure nitrogen (N_2, 99.999%). For each campaign, a blank canister was taken randomly to evaluate the analysis performance and guarantee that no target compound was detected. Air samples were collected into the vacuumed canisters through a stainless-steel line equipped with a filter (filled with glass wool and anhydrous sodium sulfate) installed at the head of the inlet. The sampling time was roughly 40 min by controlling the rate of flow until the pressure in the canister consisted with ambient pressure. After sampling, all canisters were sent to the laboratory in Shanghai Academy of Environmental Science and 105 species were analyzed within one week. The analysis methods were in accordance with the national guideline HJ759-2015 (MEP, 2015a). NMVOCs samples were concentrated in a three-stage cryofocusing preconcentration system (Model 7100A, Entech Instrument, USA) and

analyzed by a gas chromatography–mass spectrometry (GC–MS, 7890A-5975C, Agilent Instrument, USA). More details could be found in HJ759-2015 (MEP, 2015a). The method detection limits (MDLs) of 105 compounds are provided in Table S5 in the Supplement.

Before the sampling campaign, preliminary experiments were conducted to investigate the difference between on-line GC-FID measurement and canister measurements. Details are provided in Text Section S1 in the Supplement.

2.2.3. Emission estimation of NMVOCs species

The emissions of an individual NMVOCs species can be estimated based on its emission ratio (ER) to the tracer with known emissions (Warneke et al., 2007; Shao et al., 2011; Borbon et al., 2013; Wang et al., 2014; Li et al., 2019a; Simayi et al., 2020; Thera et al., 2019). It is an aggregative emission from all sources. In this study, CO was selected as the reference compound because of the following reasons. Firstly, the reactivity of CO is extremely lower than NMVOCs species and it is hardly affected by photochemical processing. Therefore the observed CO concentration could reflect its emission strength. Secondly, CO emissions show lower uncertainty compared with NMVOCs emissions (Warneke et al., 2007; Wang et al., 2014). The calculation of annual emissions for individual NMVOCs species is performed based on Eq. (4):

$$E_j = E_{CO} \times ER_j \times \frac{MW_j}{MW_{CO}} \quad (4)$$

where E_j and E_{CO} denotes the emission of species j and CO, respectively. The annual emission of CO in Nanjing was estimated at 1445.6 Gg with the uncertainty from −42% to 75% (indicated as 95% confidence interval, An et al., 2021). MW_j and MW_{CO} denote the molecular weight of species j and CO, respectively, and ER_j denotes the emission ratio of species j relative to CO (ppbv/ppmv CO). ER_j was calculated from the ambient concentration measurements, and more details about the determination and uncertainty of ERs are discussed in Text Section S2 in the Supplement.

2.3. Air quality simulation

The Models-3 Community Multi-scale Air Quality (CMAQ) v5.1 (https://www.epa.gov/cmaq/cmaq-documentation; Appel et al., 2017) coupled with the Weather Research and Forecasting (WRF) v3.7.1 (http://www.wrf-model.org/index.php; Skamarock et al., 2008) was applied to evaluate the bottom-up and the constrained NMVOCs emission estimates for Nanjing. The simulations were conducted for January, April, July and October in 2017. Three nested domains were adopted with the spatial resolutions at 27, 9 and 3 km respectively in the Lambert Conformal Conic projection centered at (110°E, 34°N). Detailed information on nested domains, model settings on meteorological simulation, chemistry mechanisms and emissions of natural origin were described in Zhao et al. (2021) and Zhou et al. (2017). The emissions of anthropogenic origin in D1 and D2 were obtained from the Multi Resolution Emission Inventory for China 2017 (MEIC, http://www.meicmodel.org/) with an original spatial resolution of 0.25° × 0.25°. The gridded MEIC emissions were aggregated to 27 km for D1, and were downscaled to 9 km for D2 according to the spatial distributions of population (for residential sources) and GDP (for other sources). For D3, the anthropogenic emissions of air pollutants except NMVOCs were obtained from An et al. (2021) with an original horizontal resolution at 4 km × 4 km and were aggregated to 3 km. NMVOCs emissions outside of Nanjing (within D3 domain) were taken from MEIC. The NMVOCs chemical species were assigned to the 2005 Carbon Bond Mechanism (CB05) to meet the requirement of CMAQ modeling. It should be noted that the NO_X emissions in the simulation were set 40% and 30% smaller than the original estimates in An et al. (2021) for January and July, respectively. CTM simulation by An et al. (2021) suggested an overestimation of NO_X emissions in the bottom-up emission inventory. Based on an inversed modeling method, moreover, Yang et al. (2021) found that the top-down estimates of NO_X emissions constrained with satellite observation were smaller than the bottom-up ones in the YRD region, especially for January and July (40% and 30%, respectively). The first 5 days were chosen as the spin-up period to provide initial conditions for later simulations.

The simulated parameters from WRF were compared with the observation dataset from China meteorological data network (http://data.cma.cn/) at 8 ground stations in D3, as summarized in Table S6 in the Supplement. The index of agreement (IOA) of temperature and relative humidity between the two datasets were larger than 0.9 and 0.7, respectively. The root mean square error (RMSE) of wind speed was smaller than 2.0. The discrepancies between two datasets were within an acceptable range (Emery et al., 2001).

3. Results and discussion

3.1. The bottom-up NMVOCs emission inventory

The anthropogenic NMVOCs emissions of Nanjing in 2017 are illustrated in Fig. 2 by source category, and the annual total emissions were estimated at 163.2 Gg. The emissions of point sources accounted for 54.5%. Compared to an estimation of biogenic VOCs (BVOCs) emissions at 28.0 Gg (Yuan et al., 2021), anthropogenic sources were the main contributors to NMVOCs emissions in the city. Solvent usage was identified as the category with the largest emissions, accounting for 42.5% of the total NMVOCs emission, followed by industrial process (33.5%) and transportation (11.4%). In sub-categories, chemical industry was the largest contributor and accounted for 36% of the industrial process emissions, followed by refining industry (25%) and plastic and rubber (22%). Traffic equipment/machinery coating and other industrial utilization such as electronics manufacturing and industrial anticorrosion, were dominating subcategories within solvent usage, accounting collectively for 70% of solvent usage emissions. The emissions from passenger cars were also noticeable and accounted for 69% of transportation sources.

As a comparison, An et al. (2021) estimated the NMVOCs emissions at 223.3 Gg while the national inventory MEIC provided a much larger value at 328.5 Gg for Nanjing in 2017. The differences resulted mainly from the various methodologies and data sources applied between studies. Different from the national and regional inventories, this study applied the procedure-based estimation method for large amount of industrial point sources, and incorporated the operating information of LDAR, the investigated NMVOCs contents in solvents, and the removal efficiencies of multiple end-of-pipe treatment facilities. The application of LDAR program changed the leak emission rate distribution and would reduce the NMVOCs emissions by 42%–57% (Ke et al., 2020). Motivated by the guidelines for the implementation of LDAR in Jiangsu Province (Zhao et al., 2020), the proportion of enterprises equipped with LDAR program reached 78% in Nanjing (Table S2 in the Supplement), leading to substantial decline of NMVOCs emissions. The solvent consumption method in this work also improved the accuracy of emission estimation as it considered the diversity in raw materials and manufacturing technologies for different enterprises. Taking automobile manufacturing industry as an example, the estimated NMVOCs emissions from an enterprise could reach 411.7 metric tons (t) based on the total vehicle production (2.42×10^5 vehicles), the uniform uncontrolled NMVOCs emission factor of 2.43 kg/vehicle (He, 2018) and the removal efficiency at 30%. With the same removal efficiency, a much smaller estimate at 56.6 t was obtained in this work based on the actual consumption of different types of solvents and the investigated NMVOCs contents in the solvents. For another enterprise with a similar annual output (1.90×10^5 vehicles), however, more comparable estimates were obtained with the two methods, i.e., 432.7 t with the emission factor method and 481.6 ton with solvent consumption method. The comparison revealed that application of uniform emission factor might neglect the difference in manufacturing technologies and emission levels between individual enterprises, as it represented the average level of available domestic measurements. As indicated in Table S3 in the Supplement, moreover, the penetration of NMVOCs control facilities was over 50% for the important

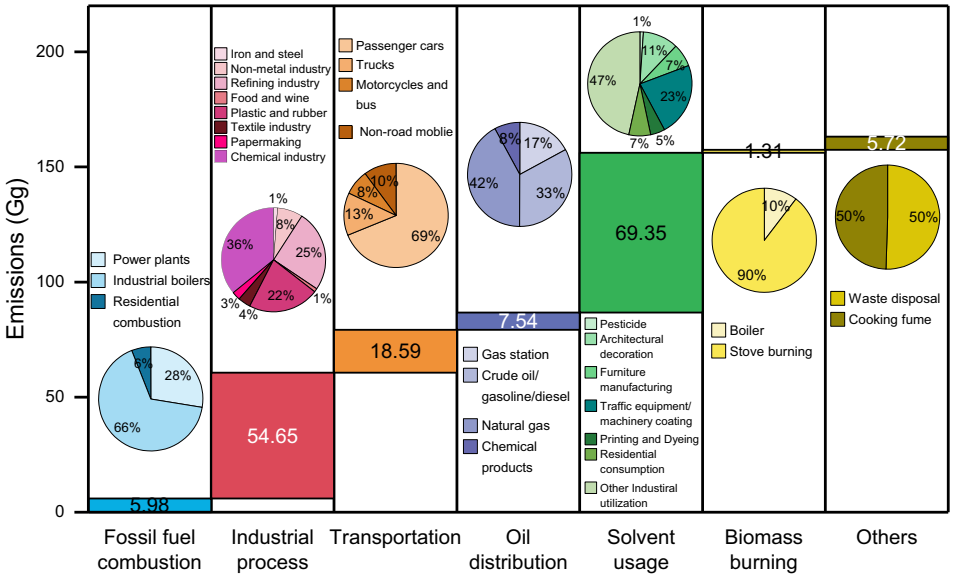

Fig. 2. The NMVOCs emissions by source category and the contributions of sub-categories to the corresponding category emissions.

NMVOCs plants in Nanjing. Compared to our previous study, the NMVOCs emissions for the city decreased from 253.4 Gg in 2014 (Zhao et al., 2017) to 163.2 Gg in 2017 (this study). The expanded use of end-of-pipe treatment facilities might be the main driving factors for the decline of NMVOCs emissions (Zhao et al., 2020).

The total emissions of NMVOCs (i.e. 163.2 Gg) were broken down into the emissions of more than 500 NMVOCs species based on the source profiles. The emissions of individual species were then grouped into 6 chemical groups. Aromatics was the group with the largest fraction to the total emissions (33.3%), followed by alkanes (25.4%) and OVOCs (20.6%). Alkenes/acetylene, halocarbons and others contributed 9.0%, 4.0% and 7.7%, respectively. The most abundant individual species included m/p-xylene (8.6%), toluene (5.1%), ethylbenzene (5.1%), ethylene (2.8%), benzene (2.8%), ethane (2.7%), ethyl acetate (2.4%), propane (2.3%), acetone (2.2%), and o-xylene (2.1%). Fig. 3 shows the emissions and source contributions by chemical group. The information of sub-categories is provided for industrial process, solvent usage and transportation. Solvent usage, especially industrial solvent-use sources such as machinery coating, furniture manufacturing, household appliances and antisepticising, was an important source of various NMVOCs species. It accounted for 59.1% and 55.9% of aromatics and OVOCs, respectively. It also contributed 37.6% of halocarbons emissions, although the fraction of halocarbons was relatively small at 4.0% in the total NMVOC emissions. Refining industry and oil distribution were the two major sources (25.7% and 14.2%, respectively) for alkanes, followed by on-road vehicles (13.0%). On-road vehicles and fossil fuel combustion made relatively big contribution to alkenes/acetylene (29.2% and 16.4%, respectively). Chemical industry was another important source of OVOCs, halocarbons and other NMVOCs, accounting for 24.1%, 25.6% and 43.1% of the emissions for the corresponding groups, respectively. Plastic and rubbers contributed significantly to halocarbons (32.2%).

Fig. 4 illustrates the spatial distributions of NMVOCs and chemical groups within a 3 km × 3 km grid system. NMVOCs emissions were mainly distributed in the central areas of Nanjing and were partly consistent with its road network. Fig. S1 in the Supplement shows the spatial distributions of selected major species ethane, ethylene, m,p-xylene and ethyl acetate, and large differences were found between species. Ethane could be emitted from various sources, such as oil distribution, gasoline cars, refining industry, domestic usage of natural gas and so on. Thus the ethane emissions were not limited in urban region but widely dispersed in the whole city.

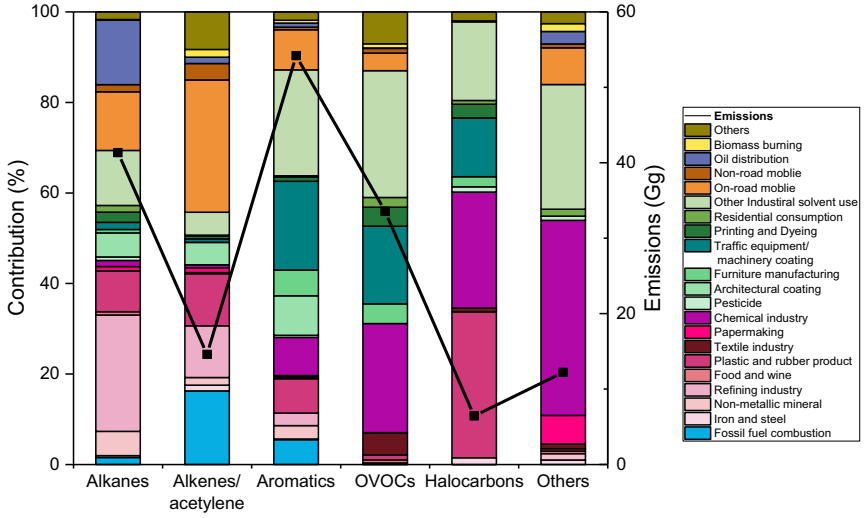

Fig. 3. The contributions of major sources to NMVOCs emissions by chemical group.

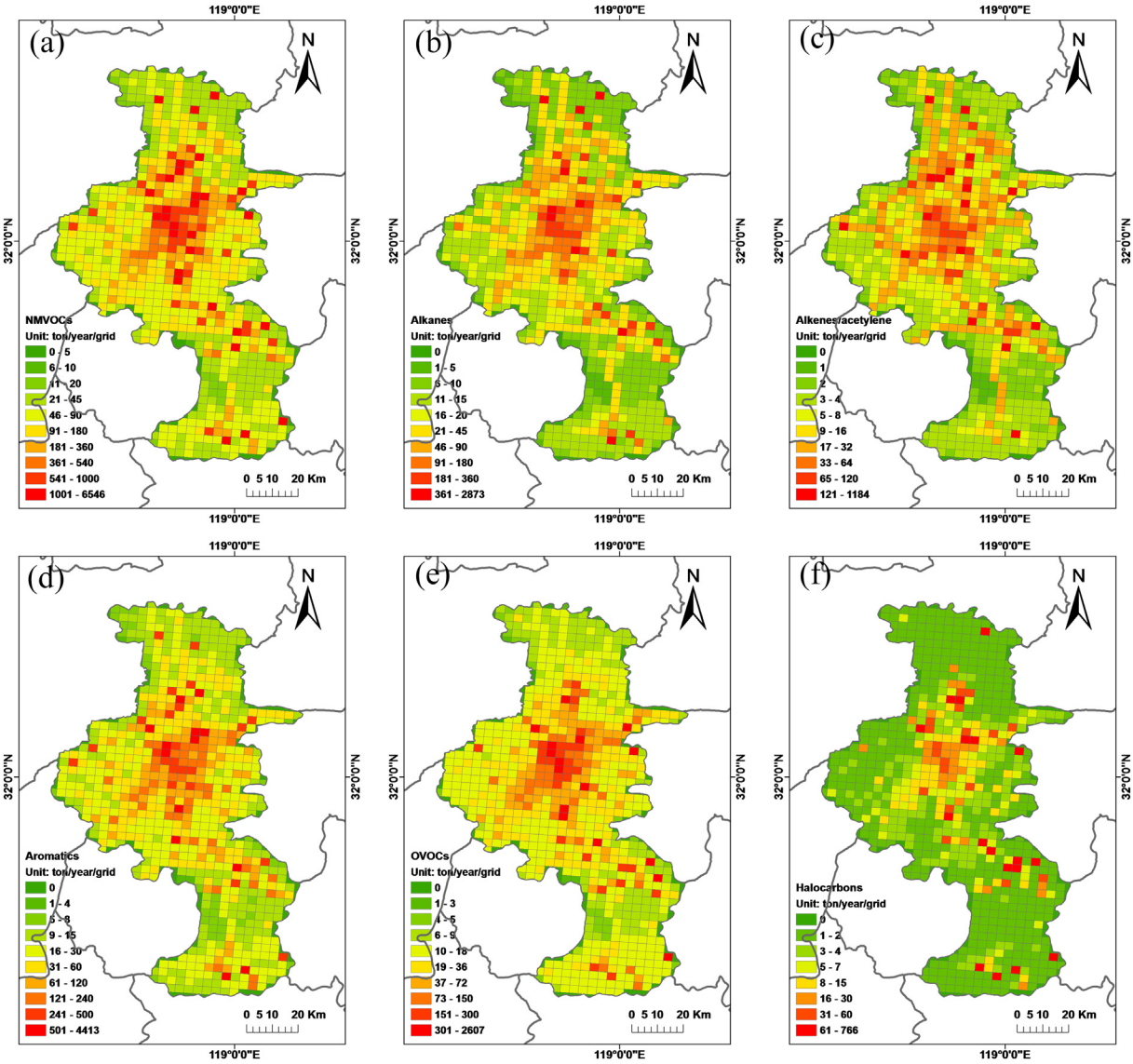

Fig. 4. Spatial distributions of NMVOCs (a), alkanes (b), alkenes/acetylene (c), aromatics (d), OVOCs (e) and halocarbons (f).

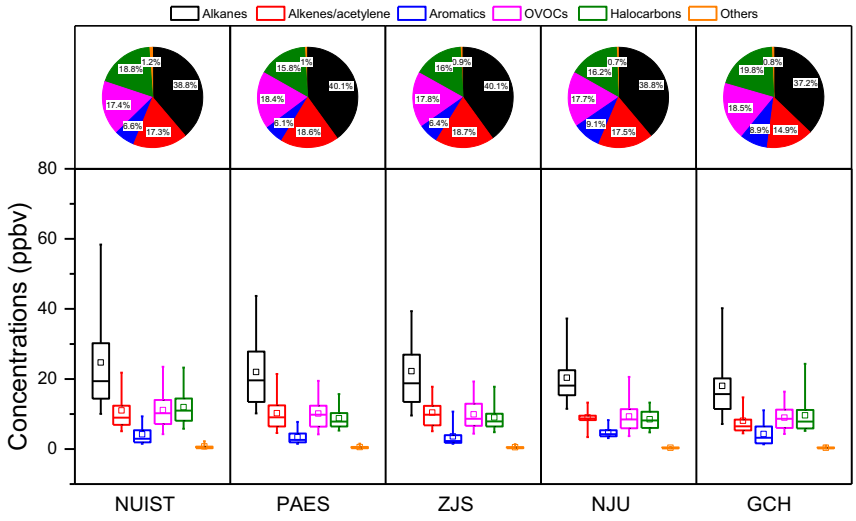

Fig. 5. The ambient levels and contributions of NMVOCs chemical groups at the five observation sites. The box and whisker indicate the ranges of 25%–75% and 5%–95%, respectively. The line and the square in the box indicate median and average level, respectively.

Abundant emissions of ethylene were found in areas with dense road network and heavy traffic flow, as on-road vehicle was the main source of ethylene. For m,p-xylene and ethyl acetate, high emissions were found in individual grids reflecting the significant contribution from industrial point sources. Fig. S2 in the Supplement compares the spatial distributions of NMVOC emissions in Nanjing for 2017 in this study and MEIC. To be consistent in resolution, MEIC was downscaled to 3 km × 3 km according to the spatial distributions of population (for residential sources) and GDP (for other sources). The results implied that downscaling of national emissions depending on certain proxies (e.g., population and economy density) might overestimate the emissions in urban areas, and could hardly catch the locations of vital point sources.

3.2. Spatiotemporal variation of NMVOCs concentrations and compositions

In this study, the highest annual mean concentration of NMVOCs was observed around industrial zones (NUIST, 63.7 ppbv) and the lowest in rural area (GCH, 48.5 ppbv). The concentrations at PAES and ZJS were comparable (55.0 and 55.6 ppbv, respectively) and slightly higher than that at NJU (52.5 ppbv). Fig. 5 exhibits the concentrations and compositions of NMVOCs chemical groups and Table 1 summarizes the ambient levels of the 20 most abundant species at each site. The concentrations of those species accounted collectively for 67.5–70.1% of the total NMVOCs. The concentrations of most NMVOCs species decreased in the following order: NUIST (industrial site) > PAES (unban site) > ZJS (city park) > NJU (suburban site) > GCH (rural site).

Among the five major chemical groups, alkanes was the most abundant group (37.2–40.1%) and ethane and propane were the most abundant species detected at all sites. Ethane and propane are the main species of natural gas and liquid petrochemical gas (Zheng et al., 2018; An et al., 2014; McCarthy et al., 2013) and come from diverse sources, such as traffic, oil and gas exploitation and residential combustion. With relatively weak atmospheric reactivity, those species have long lifetime and are easily accumulated. Therefore, the ambient levels of ethane and propane were high even in rural areas (GCH). Besides ethane and propane, typical tracers of gasoline including butane isomers and pentane isomer were also main alkane species at all sites, attributed to the contribution of gasoline vehicles and petrochemical industries.

The fractions of other groups varied at five sites. Halocarbons were the second contributor (18.8%) at NUIST with the high level of dichloromethane, indicating strong influence from industrial processes such as pharmaceutical industry. Alkenes/acetylene contributed 17.3% and the main species contained ethene, acetylene and propene. OVOCs contributed 17.4% and the main species contained ethyl acetate, and methyl methacrylate. The compositions of NMVOCs at PAES and ZJS were similar, with larger fractions of alkenes/acetylene (18.6% and 18.7%, respectively) and OVOCs (18.4% and 17.8%, respectively). Both PAES and ZJS were located in downtown areas and were more easily to be influenced by traffic emissions. Thus, the ambient levels of incompletely combusted species, such as acetylene and ethylene, would be relatively high. 2-Butanone was the most abundant OVOCs species at PAES and ZJS. It can be directly emitted from vegetation and anthropogenic activities, and can also be produced by the gas-phase oxidation of specific NMHCs such as n-butane (Yáñez-Serrano et al., 2016). Moreover, the relatively short distance (~10 km) between ZJS and PAES might not eliminate the influence of mixed air masses and the differences of NMVOCs concentrations. The fractions of alkenes/acetylene (17.5%) and OVOCs (17.7%) at NJU were slightly higher than that of halocarbons (16.2%). They consisted mainly of acetylene, ethyl acetate, propene, and dichloromethane. Halocarbons also contributed significantly (19.8%) to NMVOCs at GCH, followed by OVOCs (18.5%) and alkenes/acetylene (14.3%). The species at GCH generally have long lifetimes, such as 2-butanone and benzene, thus the remote site could be more influenced by the regional transport of emission-enriched air masses. Aromatics contributed little at the five sites but higher contributions were found at suburban and rural areas (9.1% and 8.9% at NJU and GCH, respectively) than other areas (6.1%–6.6%).

Table 1
The annual mean concentrations and standard deviations of the 20 most abundant species at five observation sites (unit: ppbv).

NUIST		PAES		ZJS		NJU		GCH	
Species	Levels	Species	Levels	Species	Levels	Species	Levels	Species	Levels
Ethane	6.56 ± 8.13	Ethane	6.19 ± 5.93	Ethane	6.13 ± 8.92	Ethane	3.98 ± 2.31	Ethane	4.55 ± 6.30
Propane	4.13 ± 2.63	Propane	4.26 ± 2.30	Propane	4.12 ± 2.22	Propane	3.08 ± 0.97	Propane	3.65 ± 2.45
Dichloromethane	3.72 ± 3.25	Acetylene	2.65 ± 1.99	2-Butanone	2.31 ± 1.32	Acetylene	2.42 ± 1.80	Methyl methacrylate	2.33 ± 2.58
Ethylene	2.78 ± 3.82	2-Butanone	2.16 ± 1.27	Acetylene	2.18 ± 0.99	Ethyl acetate	2.09 ± 1.10	Ethyl acetate	2.30 ± 1.37
Ethyl acetate	2.41 ± 1.33	Ethyl acetate	2.08 ± 0.99	Ethyl acetate	2.15 ± 1.41	i-Butane	2.08 ± 1.14	Acetylene	2.18 ± 1.22
Acetylene	2.37 ± 1.27	Ethylene	1.95 ± 2.12	Ethylene	1.88 ± 1.74	Propylene	1.92 ± 2.91	2-Butanone	1.98 ± 1.04
Methyl methacrylate	2.19 ± 2.46	Methyl methacrylate	1.86 ± 2.35	Methyl chloride	1.83 ± 1.52	n-Butane	1.87 ± 0.80	Methyl chloride	1.89 ± 0.99
Propylene	1.97 ± 3.48	Dichloromethane	1.76 ± 1.86	Methyl methacrylate	1.81 ± 1.99	i-Pentane	1.79 ± 1.15	Dichloromethane	1.86 ± 2.71
2-Butanone	1.91 ± 1.14	n-Butane	1.76 ± 0.77	n-Butane	1.78 ± 0.89	Dichloromethane	1.77 ± 1.73	Ethylene	1.73 ± 1.55
Methyl chloride	1.81 ± 1.06	Methyl chloride	1.61 ± 0.61	Dichloromethane	1.74 ± 1.98	Methylcyclopentane	1.75 ± 3.31	Toluene	1.63 ± 2.00
n-Butane	1.75 ± 0.87	i-Butane	1.60 ± 0.42	i-Butane	1.57 ± 0.45	2-Butanone	1.72 ± 1.00	n-Butane	1.59 ± 0.74
i-Butane	1.57 ± 0.40	Propylene	1.55 ± 3.05	Propylene	1.54 ± 3.44	1-Butene	1.72 ± 0.28	i-Butane	1.52 ± 0.42
Cyclohexane	1.53 ± 4.53	1-Butene	1.31 ± 0.24	1-Butene	1.33 ± 0.34	Methyl chloride	1.70 ± 0.88	1-Butene	1.22 ± 0.10
Isopropyl alcohol	1.42 ± 1.68	Toluene	1.14 ± 1.26	Toluene	1.13 ± 1.55	Methyl methacrylate	1.44 ± 1.14	n-Pentane	0.94 ± 0.37
Benzene	1.33 ± 1.68	Isopropyl alcohol	1.08 ± 0.86	n-Pentane	1.07 ± 1.08	n-Pentane	1.33 ± 0.69	Benzene	0.90 ± 1.47
Toluene	1.31 ± 1.56	n-Pentane	1.00 ± 0.41	Isoprene	1.05 ± 0.97	Toluene	1.29 ± 3.14	Isopropyl alcohol	0.85 ± 0.81
1-Butene	1.24 ± 0.22	Acrolein	0.96 ± 0.44	Acrolein	1.02 ± 0.82	Isopropyl alcohol	1.28 ± 1.75	Propylene	0.79 ± 0.25
n-Hexane	1.19 ± 1.04	Vinyl acetate	0.94 ± 1.13	Benzene	1.01 ± 1.33	Ethylene	1.19 ± 0.43	Acrolein	0.78 ± 0.35
n-Pentane	1.06 ± 0.56	Benzene	0.91 ± 0.67	n-Hexane	0.89 ± 1.80	2-Methylpentane	1.10 ± 1.07	1,2-Dichloroethane	0.66 ± 1.01
Vinyl acetate	1.02 ± 1.78	3-Methylpentane	0.78 ± 0.23	Isopropyl alcohol	0.88 ± 0.72	Vinyl acetate	1.00 ± 2.47	3-Methylpentane	0.66 ± 0.32

Fig. S3 in the Supplement illustrates the seasonal variations of NMHCs (alkanes, alkenes/acetylene and aromatics), OVOCs and halocarbons at the five sites. Similar seasonal patterns were generally found for NMHCs, with higher levels in winter and lower in summer. The seasonal variability of OH radicals, emission sources and meteorological conditions could be the key factors contributing to such differences (Wu et al., 2020). The seasonal variations of OVOCs were more complicated since they could come from both primary (biogenic and anthropogenic) and secondary sources. Similar patterns of OVOCs were found at NUIST and PAES, with the highest levels in spring/autumn followed by a slight reduction in summer and the lowest in winter. OVOCs concentrations at ZJS and NJU were also lowest in winter but comparable for the other three seasons. The elevated OVOCs concentrations in summer probably indicated the contribution from secondary formation process.

3.3. The constrained NMVOCs emissions with ground observation

3.3.1. Spatial and seasonal variations of ERs

Fig. 6 compares the ERs for the five sites. The ERs for most NMVOCs species among five sites agreed within a factor of two, with the correlation coefficient (R) from 0.89 (NUIST vs. NJU) to 0.99 (ZJS vs. PAES), indicating the similarity of NMVOCs compositions in different regions in Nanjing. Better agreement was usually found for alkanes and halocarbons, with R larger than 0.90 and worse agreement for alkenes/acetylene and aromatics, with the lowest R at 0.68 (GCH vs. NJU for aromatics). Moreover, we calculated relative standard deviation (RSD) for ERs among five sites and found it was lower than 30% for 59 species, and lower than 40% for 79 species. The ER for tetrahydrofuran at NUIST was 3.5–6.1 times higher than that determined at other sites, implying the larger emissions of tetrahydrofuran around industrial zones. However, inconsistent spatial distribution of tetrahydrofuran emissions was found in the bottom-up emission inventory and higher emissions existed in the regions where PAES and ZJS were located. According to the source profiles used in this study, tetrahydrofuran was not mainly from industrial sources but commercial/consumer solvent use, diesel vehicle and biomass burning, and it was thus allocated in the downtown areas. In contrast, a recent study reported high mass fraction of tetrahydrofuran (8.4%) in the NMVOCs emissions from water-based coating industry (Li et al., 2018). Given the ongoing shift from organic solvent to water-soluble solvent usage in China, therefore, current source profiles might probably underestimate the tetrahydrofuran emission from coating industry. Another example was the higher ERs for i-pentane and ethylbenzene at NJU than other sites, attributed probably to the influence from the nearby oil refinery plant (at a distance of 5 km). The ERs for propene, 1-butene and 1-pentene at other sites were generally higher than those at NJU. As the observation data at 9:00 am were only applied to calculate the ERs at other sites to limit the influence of photochemical processing (see Text Section S2 in the Supplement), the heavy traffic in rush hour was expected to elevate the concentrations and thereby ERs of C3–C5 alkenes.

Seasonal variations of ERs in Nanjing were investigated and Fig. S4 in the Supplement illustrates the ERs for four seasons. The ERs for most NMVOCs species in four seasons generally agreed within a factor of two, with R from 0.80 (winter vs. summer) to 0.96 (autumn vs. spring). There were also some species showing greater variability. Clear discrepancies were found for OVOCs and alkenes/acetylene between summer and winter (Fig. S4e). ERs for some halocarbons were generally higher in spring (Fig. S4a–c). These results might be caused by the uncertainties of ERs (mainly for OVOCs) or emission sources. Temporal variations of emissions will be further discussed in Section 3.3.3.

3.3.2. The annual emissions of individual NMVOCs species

With the averaged ERs and corresponding standard deviations (SDs) at the five sites, the annual emissions of each species were constrained for Nanjing along with uncertainties. The total emissions of 105 species

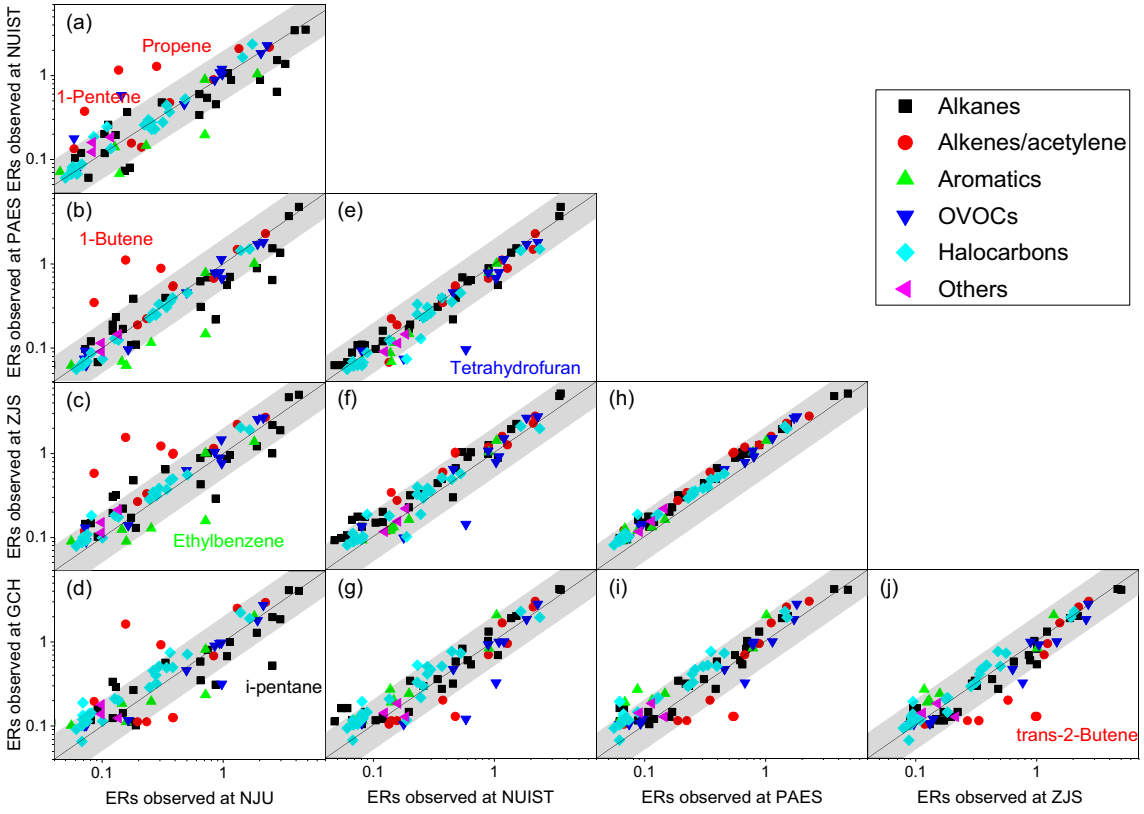

Fig. 6. Comparisons of ER for individual species determined at the five site: (a) NUIST vs. NJU, (b) PAES vs. NJU, (c) ZJS vs. NJU, (d) GCH vs. NJU, (e) PAES vs. NUIST, (f) ZJS vs. NUIST, (g) GCH vs. NUIST, (h) ZJS vs. PAES, (i) GCH vs. PAES, and (j) GCH vs. ZJS. The black line represents the 1:1 line and the grey area represents the uncertainty range of ±100%.

(NMVOCs-105) were aggregated to 195.6 Gg with the ground observation constraints, 81.1% larger than the estimate of 108.0 Gg for NMVOCs-105 in the bottom-up emission inventory. Fig. 7 compares the emissions of individual NMVOCs species between the two estimates. The uncertainties of constrained emissions were large for i-pentane, i-butane, 1-butene, toluene, ethylacetate and dichloromethane, due to the spatial discrepancies of ERs among different sites. The annual emissions for 48 NMHCs species between the constrained and bottom-up estimates agreed within a factor of four, and 23 NMHCs species agreed within a factor of two. The discrepancies for OVOCs and halocarbons were much larger. As discussed in Text Section S2 in the Supplement, the ERs might be slightly overestimated due to the absence of nighttime data and it could partly explain the discrepancies. Moreover, the discrepancies indicated the possible uncertainties of the bottom-up emission inventory. For example, the emissions of propane, n-butane, i-butane and acetylene in the constrained estimates were 8.8, 5.8, 5.7, and 3.3 Gg respectively, 2.3–3.2 times of those in the bottom-up emission inventory. The constrained emissions of most alkenes were also larger than the bottom-up estimates. The higher emissions of propane and butane along with acetylene in the constrained estimates probably implied an underestimation of the transportation emissions in the bottom-up inventory. Propane and butane are important tracers of natural gas and gasoline, and acetylene is mainly from incomplete combustion sources. They are all related to vehicle emissions. Another evidence was the smaller contribution of transportation in the bottom-up emission inventory (11.4%) than that from source apportionment study with the Positive Matrix Factorization (PMF) method (23.5%, Wu et al., 2020). Due to insufficient real time traffic flow within the city, the NMVOCs emissions of on-road vehicles were estimated based on vehicle population, which could ignore the emissions from the vehicles passing through but not registered in the city. Besides, the uncertainty of the bottom-up estimate could also be enhanced as the influences of the changed fuel quality and road condition were not dynamically considered in the emission calculation attributed to the limited data.

The emission levels of ethylbenzene and m/p-xylene from the ground measurement constraining were 80.9% and 93.3% smaller than those in the bottom-up inventory respectively, and it resulted probably from the uncertainties in the source profiles. Aromatics came largely from solvent utilization processes in Nanjing, including machinery coating, automobile coatings and other industrial solvent usage (Fig. 3). The NMVOCs species profiles of those sources were mainly compiled based on measurement results of organic solvents. As mentioned earlier, application of water-soluble solvents instead of organic solvents was encouraged to control NMVOCs recently (Zhao et al., 2020), and a much smaller fraction of aromatics was found in water-soluble solvents (11.3%) than organic solvents (52.3–71.5%) (Li et al., 2018).

The annual emissions of many OVOCs and halocarbons were much lower in the bottom-up inventory than those from measurement constraining. For example, the emission of tetrahydrofuran constrained by the measurements was 0.8 Gg, 98.7 times of that determined by the bottom-up emission inventory. The emissions of dichloromethane and 1,1,1-trichloroethane were 8.2 and 1.1 Gg respectively in the constrained estimates and were 1.5 and 0.008 Gg respectively in the bottom-up emission inventory. Similar results were also found in Beijing (Li et al., 2019a) and Chengdu (Simayi et al., 2020). One possible explanation is that the secondary formation is a critical source of OVOCs in ambient air, as shown in the spatiotemporal variations of observed OVOCs. Due to the limitation of ER method, secondary formation of OVOCs through photochemical oxidation could not be fully excluded (Text Section S2 in the Supplement). Moreover, the uncertainty in current source profiles contributed partly to the inconsistency as well. As most of the domestic measurements focused on the NMHC species (Mo et al., 2016), the mass fractions of OVOCs and halocarbons in the total NMVOCs could be underestimated. Besides, due to the insufficient coverage of source categories by domestic measurement studies, information from foreign databases was adopted such as the Organic Gas and PM Speciation Profiles of Air Pollution Sources (SPECIATE, USEPA, 2014). However, SPECIATE excludes NMVOCs species with low atmospheric photochemical reactivity, including dichloromethane, 1,1,1-trichloroethane, and fluorochemicals (Li et al., 2019a). The inconsistency between the constrained and bottom-up emission estimates suggested the necessity of further field measurement studies on source profiles of NMVOCs.

3.3.3. Evaluation of monthly variations

Based on the monthly average ERs and monthly emissions of CO, the NMVOCs emissions of 105 observed species were calculated for the 12 months within 2017. Fig. 8 compares the monthly variations of emissions between the bottom-up and constrained estimates. The NMVOCs emissions varied from 7.9 Gg in February to 10.6 Gg in December in the bottom-up inventory, with insignificant monthly variations. However, the largest emissions of NMVOCs were found in April (20.0 Gg) and September

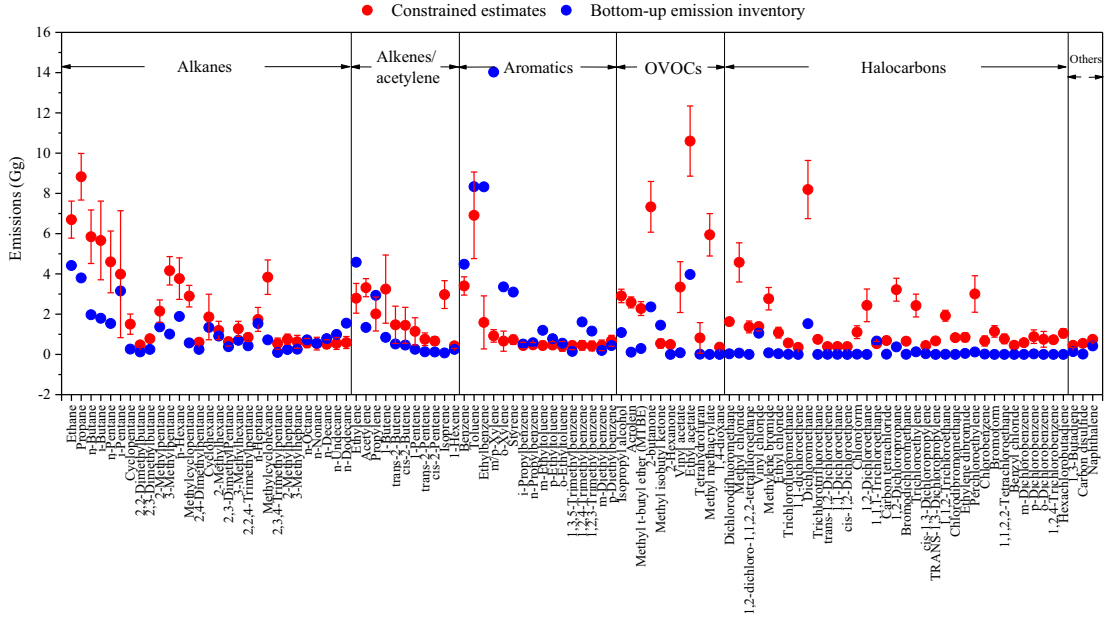

Fig. 7. The emissions of individual NMVOCs species from the bottom-up inventory and ground measurement constraining. The error bar represents for uncertainties derived from SDs of ERs.

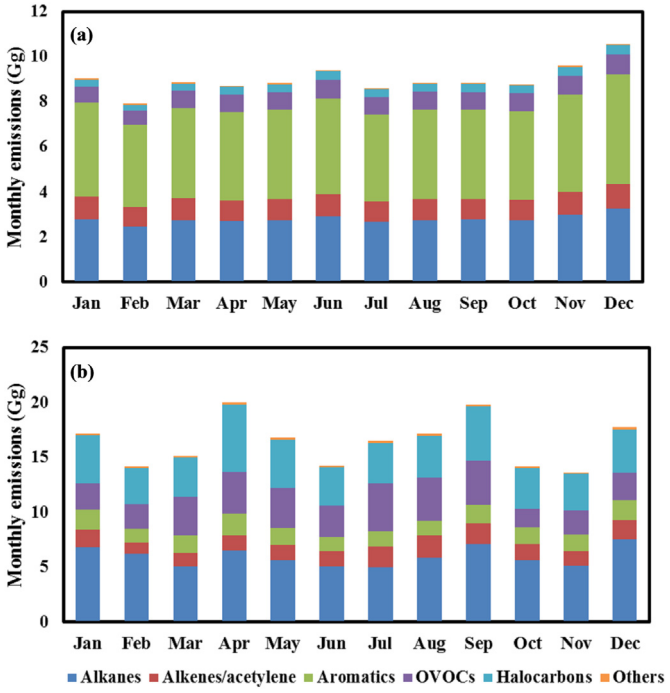

Fig. 8. The monthly emissions of 105 observed NMVOCs species (presented as chemical groups) from the bottom-up (a) and the constrained emission estimates (b).

(19.8 Gg) in the constrained estimates. The discrepancies of monthly variations between two estimates indicated the uncertainty of monthly allocation of NMVOCs emissions with bottom–up method. Facing severe O_3 pollution during summer time, high NMVOCs-emitted sources are required to be shut down and might result in a decrease of NMVOCs emissions. Such monthly variations could not be caught by the bottom-up emission inventory. It should be noted that uncertainties probably existed in constrained estimates. The higher OVOCs emissions were found in warm seasons (e.g. from March to September) than the bottom-up inventory, as current ER calculation method could not completely remove the influence of secondary aerosol formation. The higher alkenes and acetylene emissions from July to September resulted partly from the relatively strong biogenic emissions (e.g., isoprene) in summer that were not included in the current bottom-up inventory.

3.4. Evaluation of NMVOCs emissions through air quality modeling

Air quality modeling was conducted based on the monthly NMVOCs emissions from the bottom-up and the constrained emission inventory respectively. For the latter, the monthly emissions of the 105 observed species were changed with the constrained estimates in Nanjing, while the emissions of other species, and the spatial distribution and category contribution remained the same as the bottom-up inventory. Statistical indicators including the mean normal bias (MNB), mean normal bias error (MNE), normalized mean bias (NMB), and normalized mean error (NME) were applied to compare the WRF-CMAQ simulation and ground observations of daily maximum 8 h O_3 concentrations (MDA8). The ground observation data of O_3 were collected at 9 state-operated monitoring sites in Nanjing (https://data.epmap.org). Table 2 compares the model performance with the bottom-up and constrained emission estimates for Nanjing. Applications of the both two inventories led to underestimation in O_3 simulation except for July, while the underestimation was slightly corrected with the constrained emissions. Based on the bottom-up emission inventory, the MNBs for Nanjing were calculated at −17.1%, −6.4%, 12.7% and −2.0%, and the MNEs were 37.1%, 23.3%, 27.1% and 22.2% for January, April, July and October, respectively. The analogous numbers were −16.5%, −5.3%, 14.3% and −1.2% for MNBs, and 37.0%, 23.0%, 27.2% and 22.1% for MNEs, respectively, when the constrained emission estimates were applied in the simulation. Most of MNB and MNE values were within the criteria (MNB ≤ ±15%, MNE ≤ 30%) suggested by USEPA (2005) in the two cases. Compared to bottom-up inventory, model performance of O_3 simulation was slightly improved when the constrained estimates were applied.

With detailed information on individual sources incorporated as much as possible, the bottom-up emission inventory developed in this work improved the emission estimates and spatial distributions of NMVOCs emissions, resulting in satisfying model performance of O_3 simulation. A review study shown that NMB values in 53% of studies in China were out of range at ±15%, and 22% were out of range at ±30% (Yang et al., in preparation). The NMBs values in this study were within ±15% except for January, better than most of previous studies. Furthermore, the slightly improved O_3 simulation with the constrained estimates indicates the combined effect of emission changes for the observed 105 species. Fig. S5 in the Supplement compares the emissions of CB05 species in the bottom-up emission inventory and constrained estimates for the four month. The constrained estimates were 30–56% and 59–72% smaller for TOL and XYL but 56–248% and 125–243% larger for OLE and IOLE than the bottom-up emission inventory. The limited change in the simulated O_3 concentration could result from the offset influence of the reduction of TOL and XYL emissions and the increment of OLE and IOLE in the constrained inventory.

Uncertainties of NMVOCs emissions outside of Nanjing would affect the results as well since O_3 is a secondary pollutant and can be transport from nearby cities. To quantify this impact, we conducted a sensitive analysis with NMVOCs emissions constrained in the whole D3 domain. Compared to the bottom-up emission inventory, the absolute values of MNB changed 3.8–8.5% for different months when NMVOCs emissions were constrained in the whole D3 domain, larger than those when NMVOCs emissions were only constrained in Nanjing (0.6–1.6%, Table 2). It implied that the uncertainties of NMVOCs emissions from nearby cities would affect the results. It should be noted that bias existed in application of observations in Nanjing to constrain NMVOCs emissions from nearby cities as well. More

Table 2
The model performance of MDA8 with the bottom-up and constrained inventory for January, April, July and October 2017 in Nanjing. The values in bold represent for better performance with constrained inventory.

	MEAN OBS (μg/m^3)	Bottom-up						Constrained					
		MEAN SIM (μg/m^3)	MNB (%)	MNE (%)	NMB (%)	NME (%)	R	MEAN SIM (μg/m^3)	MNB (%)	MNE (%)	NMB (%)	NME (%)	R
January	70.9	53.6	−17.1	37.1	−24.5	37.2	0.26	53.9	**−16.5**	**37.0**	**−24.0**	**37.0**	**0.27**
April	132.6	116.5	−6.4	23.3	−12.1	22.5	0.57	117.9	**−5.3**	**23.0**	**−11.0**	**22.0**	**0.58**
July	139.0	141.3	12.7	27.1	1.7	21.4	0.66	143.6	14.3	27.2	3.4	**21.2**	**0.67**
October	103.1	96.2	−2.0	22.2	−6.7	21.3	0.67	96.9	**−1.2**	**22.1**	**−6.1**	**21.1**	0.67

Note: MNB, MNE, NMB and NME were calculated as the following equations (S_i and O_i indicate the results from modeling simulation and observation, respectively):

$$\mathrm{MNB} = \frac{1}{N}\sum_{i=1}^{n}\left(\frac{S_i - O_i}{O_i}\right) \times 100\%;\ \mathrm{MNE} = \frac{1}{N}\sum_{i=1}^{n}\left|\frac{S_i - O_i}{O_i}\right| \times 100\%;\ \mathrm{NMB} = \frac{\sum_{i=1}^{n}(S_i - O_i)}{\sum_{i=1}^{n} O_i} \times 100\%;\ \mathrm{NME} = \frac{\sum_{i=1}^{n}|S_i - O_i|}{\sum_{i=1}^{n} O_i} \times 100\%.$$

measurements were recommended to be conducted and published for constraining NMVOCs emissions effectively in the future.

The negative values of MNBs shown that NMVOCs emission inventories in this study were still likely an underestimation of the actual emissions. Moreover, besides NMVOCs, the NO_X emissions would also influence the O_3 simulation. We evaluated the NO_2 simulations and the NMB values of 24%, 11%, 15% and 20% were found for January, April, July and October, respectively. The result implied that the NO_X emissions might still be overestimated although it has been adjusted based on the analysis with the top-down method by Yang et al. (2021). To explore the sensitivity of O_3 formation to its precursor emissions, two cases were set for January and July respectively: the NMVOCs-abatement case with 30% reduction of NMVOCs emissions in D3 domain, and the NO_X-abatement case with 30% reduction of NO_X in D3 domain. The base scenarios were set with constrained emission inventory. The temporal changes of simulated MDA8 between case scenarios and base scenarios at 9 state-operated monitoring sites in Nanjing are illustrated in Fig. S6 in the Supplement. Both in winter and summer, simulated MDA8 were decreased once the NMVOCs emissions declined. In contrast, concentrations were generally elevated with the NO_X emission reduction with exceptions on some summer days. The monthly mean MDA8 declined by 2.6% and 3.3% with 30% NMVOCs emissions off in January and July respectively, while it would increase by 13.1% and 1.5% with 30% NO_X emissions off in January and July respectively. The result implied that O_3 formation mechanism in Nanjing was generally NMVOC-limited and turned transitional on some days in summer. Therefore, the overestimation of O_3 simulation in summer and underestimation of O_3 simulation in other seasons could be partly attributed to the overestimation of NO_X emissions.

The overestimation of simulated O_3 in July could result from the uncertainty in the chemical mechanism of the model as well. It was reported that reduced cloudiness and attenuation of photolysis in CMAQ 5.2 generally resulted in higher O_3 mixing ratios (Appel et al., 2017). Li et al. (2019b) conducted an intercomparison of surface O_3 simulation from 14 chemical transport models and implied that the larger overestimation of summer O_3 than winter for eastern China resulted possibly from the uncertainty in the photochemical treatment in model. The uncertainties of planetary boundary layer and vertical transport might also be the reason for higher O_3 simulation in July (Akimoto et al., 2019; Zhao et al., 2019).

3.5. Species-based OFP and implications for ozone control strategy

Local governments in China have strengthened several strategies to minimize NMVOCs pollution from vehicle and industrial emissions in recent years, but most of those policies focused particularly on lowering the total emissions of NMVOCs (Zhao et al., 2020). Given the diverse reactivities in O_3 formation for different NMVOCs species, the reactivity-based control is more effective and efficient than the emission-based approach. From the perspective of reactivity-based control, high OFP-contributing species would be targeted with priority instead of high emission-contributing species. The OFP of individual NMVOCs is calculated by the product of its emission amount and its MIR (maximum incremental reactivity) value (Carter, 2010). Fig. S7 in the Supplement provides OFP contributions of different chemical groups based on the bottom–up emission inventory and the constrained estimates respectively. In the bottom-up inventory, aromatics and alkenes/acetylene were identified as the main contributors, accounting for 50.9% and 24.6% of the total OFPs, respectively. With the constrained estimates incorporated, however, alkenes/acetylene became the largest contributor (33.3%), followed by OVOCs (24.2%) and aromatics (19.5%). The top 15 contributing species to the OFPs changed as well, as shown in Table S7 in the Supplement. Totally 12 species were suggested as the priority for O_3 pollution control in Nanjing. Besides 6 common species in the two emission estimates (i.e. ethylene, propylene, toluene, 1-butene, trans-2-butene and cis-2-butene), 3 highest OFP species in the bottom-up emission inventory (i.e. m/p-xylene, o-xylene and ethylbenzene) and 3 highest OFP species in the constrained estimates (i.e. acrolein, vinyl acetate and 1-pentene) were selected. Note that methyl methacrylate and isoprene were excluded since they might be affected by the secondary formation and biogenic sources respectively in the constrained estimates (Li et al., 2019a; Mochizuki et al., 2015).

Fig. 9 illustrates the OFP contributions from different source categories for the 12 species with priority of emission control. Surface coating such as machinery coating, furniture manufacturing, and household appliances made significant contributions to toluene, ethylbenzene, m/p-xylene and o-xylene (49.5–83.8%). Fossil fuel combustion (25.1%), others (mainly refuse incineration, 23.9%), and on-road vehicles (22.6%) were the major sources of ethylene. Oil exploitation and refinery dominated the OFPs of trans-2-butene (62.7%), and also contributed considerably to cis-2-butene (32.8%), 1-butene (25.0%), and propylene (23.5%). Plastic and rubber production contributed 37.3% to propylene OFP. On-road vehicles and chemical industry dominated the OFPs of acrolein (59.9%) and vinyl acetate (72.0%) respectively. Overall, solvent use sources, on-road vehicles, industrial process including oil exploitation and refinery and plastic and rubber product, and fossil fuel combustion contributed significantly to the high OFP-contributing species.

Enhanced measures involving are suggested for control of NMVOCs emissions, including cleaner production processes and more stringent end-of-pipe approaches. For example, the use of closed integrated production technology is recommended to reduce the fugitive emission. Organic

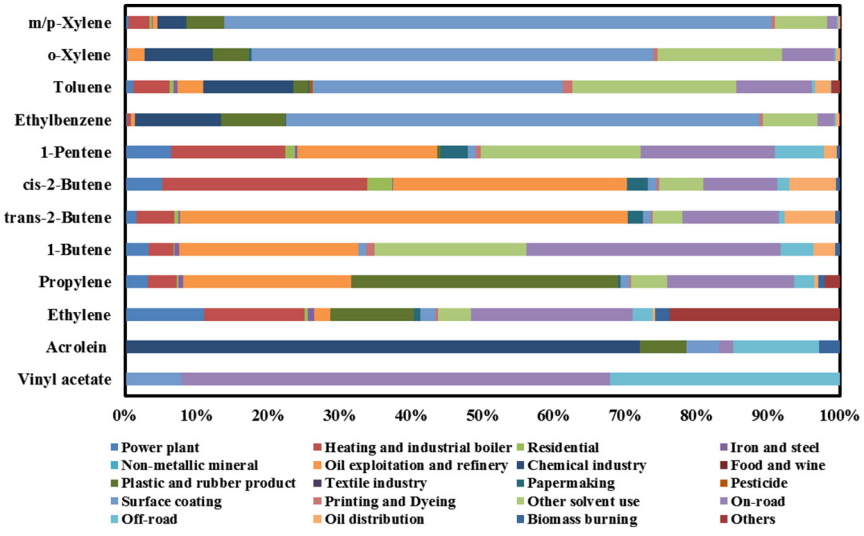

Fig. 9. The contributions of different sources to the OFP for the 12 NMVOCs species with emission control priority.

solvents should be increasingly replaced with water-based coatings or high solid coatings. Besides, end-of-pipe treatment facilities were not covered comprehensively and the operation and maintenance differed significantly among various enterprises, and further improvement on penetration and supervision of those facilities is needed.

4. Conclusion

Efforts have been made to reconcile the bottom-up methodology and ground measurement constraints to improve the city-scale NMVOCs emission inventory in this study. The total NMVOCs emissions in Nanjing were estimated at 163.2 Gg for 2017 based on a refined bottom-up methodology, which incorporated the procedure-based method and best available information of manufacturing technologies, materials and products, operation and maintenance, and end-of-pipe treatment facilities for individual sources. Solvent usage, industrial process and transportation were the top three NMVOCs sources, accounting for 42.5%, 33.5%, and 11.4% of the total emissions, respectively. Aromatics was the group with the largest fraction to the total emissions (33.3%). Ground measurements of 105 NMVOCs species were conducted at five sites representing different functional zones in Nanjing and the spatiotemporal pattern of NMVOCs compositions were analyzed. The highest annual mean concentration of NMVOCs was observed around industrial zones and the lowest in rural area. Alkanes was the most abundant group at all sites (37.2–40.1%). With an ER method based on the observation of NMVOCs species and the tracer CO, the total emissions of the NMOVCs-105 were constrained at 195.6 Gg, 81.1% larger than the bottom-up estimate (108.0 Gg for NMOVCs-105). The constrained species-specific emission data indicated an overestimation of aromatics and underestimation of OVOCs and halocarbons in the bottom-up emission inventory. Satisfying model performances were achieved in O_3 simulation with WRF-CMAQ based on the both emission estimates. The MNBs and MNEs were generally within the criteria suggested by USEPA. The model performance was improved with the constrained estimates due to a combined effect of the changed emissions of the 105 observed species. Combining the constrained emission estimates, the top 12 OFP-contributing species were suggested as the priority for O_3 pollution control, mainly C2–C4 alkenes and C7–C9 aromatics. Surface coating, on-road vehicles, and oil exploitation and refinery were identified as the target sources for O_3 reduction, from a perspective of reactivity-based control. The results provide a more scientific guide for NMVOCs emission control and O_3 pollution alleviation for developed cities.

CRediT authorship contribution statement

Rongrong Wu: Methodology, Investigation, Data curation, Visualization, Writing – original draft, Writing – review & editing. **Yu Zhao:** Supervision, Methodology, Writing – review & editing, Project administration, Funding acquisition. **Sijia Xia:** Resources, Methodology. **Wei Hu:** Resources. **Fangjian Xie:** Resources, Methodology. **Yan Zhang:** Methodology. **Jinjin Sun:** Resources. **Huan Yu:** Resources. **Junlin An:** Resources. **Yutong Wang:** Resources.

Declaration of competing interest

The authors declare that they have no known competing financial interests or personal relationships that could have appeared to influence the work reported in this paper.

Acknowledgements

This work received support from the Natural Science Foundation of China (41922052 and 42177080) and the Jiangsu Provincial Fund on $PM_{2.5}$ and O_3 Pollution Mitigation (No. 2019023). We also thank the Qingyue Open Environmental Data Center (https://data.epmap.org) for its support on air quality data and thank Prof. Jianlin Hu and Prof. Xinlei Ge for their help on the samplings of NMVOCs and dataset of CO.

Appendix A. Supplementary data

Supplementary data to this article can be found online at https://doi.org/10.1016/j.scitotenv.2021.152447.

References

Akimoto, H., Nagashima, T., Li, J., Fu, J.S., Ji, D.S., Tan, J.N., Wang, Z.F., 2019. Comparison of surface ozone simulation among selected regional models in MICS-Asia III - effects of chemistry and vertical transport for the causes of difference. Atmos. Chem. Phys. 19, 603–615. https://doi.org/10.5194/acp-19-603-2019.

An, J., Huang, Y., Huang, C., Wang, X., Yan, R., Wang, Q., Wang, H., Jing, S.A., Zhang, Y., Liu, Y., Chen, Y., Xu, C., Qiao, L., Zhou, M., Zhu, S., Hu, Q., Lu, J., Chen, C., 2021. Emission inventory of air pollutants and chemical speciation for specific anthropogenic sources based on local measurements in the Yangtze River Delta region, China. Atmos. Chem. Phys. 21, 2003–2025. https://doi.org/10.5194/acp-21-2003-2021.

An, J., Zhu, B., Wang, H., Li, Y., Lin, X., Yang, H., 2014. Characteristics and source apportionment of VOCs measured in an industrial area of Nanjing, Yangtze River Delta. China. Atmos. Environ. 97, 206–214. https://doi.org/10.1016/j.atmosenv.2014.08.021.

Appel, K.W., Napelenok, S.L., Foley, K.M., Pye, H.O.T., Hogrefe, C., Luecken, D.J., Bash, J.O., Roselle, S.J., Pleim, J.E., Foroutan, H., Hutzell, W.T., Pouliot, G.A., Sarwar, G., Fahey, K.M., Gantt, B., Gilliam, R.C., Heath, N.K., Kang, D., Mathur, R., Schwede, D.B., Spero, T.L., Wong, D.C., Young, J.O., 2017. Description and evaluation of the community multiscale air quality (CMAQ) modeling system version 5.1. Geosci. Model Dev. 10, 1703–1732. https://doi.org/10.5194/gmd-10-1703-2017.

Atkinson, R., 2000. Atmospheric chemistry of VOCs and NOx. Atmos. Environ. 34, 2063–2101. https://doi.org/10.1016/S1352-2310(99)00460-4.

Borbon, A., Gilman, J.B., Kuster, W.C., Grand, N., Chevaillier, S., Colomb, A., Dolgorouky, C., Gros, V., Lopez, M., Sarda-Esteve, R., Holloway, J., Stutz, J., Petetin, H., McKeen, S., Beekmann, M., Warneke, C., Parrish, D.D., De Gouw, J.A., 2013. Emission ratios of anthropogenic VOC in northern mid-latitude megacities observations vs. Emission inventories in Los Angeles and Paris. J. Geophys. Res. Atmos. 118, 2041–2057. https://doi.org/10.1002/jgrd.50059.

Carter, W.P., 2010. Updated maximum incremental reactivity scale and hydrocarbon bin reactivities for regulatory applications. Report to California Air Resources Board Contract.

Chen, D., Cui, H.F., Zhao, Y., Yin, L.N., Lu, Y., Wang, Q.G., 2017. A two-year study of carbonaceous aerosols in ambient PM2.5 at a regional background site for western Yangtze River Delta, China. Atmos. Res. 183, 351–361. https://doi.org/10.1016/j.atmosres.2016.09.004.

Emery, C., Tai, E., Yarwood, G., 2001. Enhanced meteorological modeling and performance evaluation for two Texas episodes. Report to the Texas Natural Resources Conservation Commission.

USEPA (U.S. Environmental Protection Agency), 2005. Guidance on the Use of Models and Other Analyses in Attainment Demonstrations for the 8-hour Ozone NAAQS, EPA-454/R-05-002.

Fu, T.M., Jacob, D.J., Palmer, P.I., Chance, K., Wang, Y.X., Barletta, B., Blake, D.R., Stanton, J.C., Pilling, M.J., 2007. Space-based formaldehyde measurements as constraints on volatile organic compound emissions in east and South Asia and implications for ozone. J. Geophys. Res. Atmos. 112, D06312. https://doi.org/10.1029/2006JD007853.

Guenther, A., Karl, T., Harley, P., Wiedinmyer, C., Palmer, P.I., Geron, C., 2006. Estimates of global terrestrial isoprene emissions using MEGAN (Model of emissions of gases and aerosols from Nature). Atmos. Chem. Phys. 6, 3181–3210. https://doi.org/10.5194/acp-6-3181-2006.

Guo, H., Ling, Z.H., Cheng, H.R., Simpson, I.J., Lyu, X.P., Wang, X.M., Shao, M., Lu, H.X., Ayoko, G., Zhang, Y.L., Saunders, S.M., Lam, S.H.M., Wang, J.L., Blake, D.R., 2017. Tropospheric volatile organic compounds in China. Sci. Total Environ. 574, 1021–1043. https://doi.org/10.1016/j.scitotenv.2016.09.116.

He, K.B. (Ed.), 2018. Guidebook of Air Pollutant Emission Inventory Development for Chinese Cities (in Chinese). Beijing, China.

Hu, R., Liu, G., Zhang, H., Xue, H., Wang, X., 2018. Levels, characteristics and health risk assessment of VOCs in different functional zones of Hefei. Ecotoxicol. Environ. Saf. 160, 301–307. https://doi.org/10.1016/j.ecoenv.2018.05.056.

Janssens-Maenhout, G., Crippa, M., Guizzardi, D., Dentener, F., Muntean, M., Pouliot, G., Keating, T., Zhang, Q., Kurokawa, J., Wankmüller, R., Denier van der Gon, H., Kuenen, J.J.P., Klimont, Z., Frost, G., Darras, S., Koffi, B., Li, M., 2015. HTAP_v2.2: a mosaic of regional and global emission grid maps for 2008 and 2010 to study hemispheric transport of air pollution. Atmos. Chem. Phys. 15, 11411–11432. https://doi.org/10.5194/acp-15-11411-2015.

Karl, T., Apel, E., Hodzic, A., Riemer, D.D., Blake, D.R., Wiedinmyer, C., 2009. Emissions of volatile organic compounds inferred from airborne flux measurements over a megacity. Atmos. Chem. Phys. 9, 271–285. https://doi.org/10.5194/acp-9-271-2009.

Ke, J., Li, S., Zhao, D., 2020. The application of leak detection and repair program in VOCs control in China's petroleum refineries. J. Air Waste Manag. Assoc. 70, 862–875. https://doi.org/10.1080/10962247.2020.1772407.

Li, J., Hao, Y., Simayi, M., Shi, Y., Xi, Z., Xie, S., 2019a. Verification of anthropogenic VOC emission inventory through ambient measurements and satellite retrievals. Atmos. Chem. Phys. 19, 5905–5921. https://doi.org/10.5194/acp-19-5905-2019.

Li, J., Nagashima, T., Kong, L., Ge, B., Yamaji, K., Fu, J.S., Wang, X., Fan, Q., Itahashi, S., Lee, H.-J., Kim, C.-H., Lin, C.-Y., Zhang, M., Tao, Z., Kajino, M., Liao, H., Li, M., Woo, J.-H., Kurokawa, J., Wang, Z., Wu, Q., Akimoto, H., Carmichael, G.R., Wang, Z., 2019b. Model evaluation and intercomparison of surface-level ozone and relevant species in East Asia in the context of MICS-Asia phase III – part 1: overview. Atmos. Chem. Phys. 19, 12993–13015. https://doi.org/10.5194/acp-19-12993-2019.

Li, M., Zhang, Q., Zheng, B., Tong, D., Lei, Y., Liu, F., Hong, C., Kang, S., Yan, L., Zhang, Y., Bo, Y., Su, H., Cheng, Y., He, K., 2019c. Persistent growth of anthropogenic non-methane volatile organic compound (NMVOC) emissions in China during 1990–2017: drivers, speciation and ozone formation potential. Atmos. Chem. Phys. 19, 8897–8913. https://doi.org/10.5194/acp-19-8897-2019.

Li, X., Su, W., Li, B., Long, M., Li, L., Zhang, Z., Yu, Y., Wang, Y., Wang, X., 2018. Source profiles and chemical reactivity of volatile organic compounds from surface coating of aluminum products in Foshan, China. Huanjing Kexue 39 (12), 5334–5343. https://doi.org/10.13227/j.hjkx.201803224.

Liang, X., Sun, X., Lu, Q., Ren, L., Liu, M., Su, Y., Wang, S., Lu, H., Gao, B., Zhao, W., Sun, J., Gao, Z., Chen, L., 2021. VOC emission inventory of architectural coatings and adhesives for new buildings in China based on investigated and measured data. Atmos. Environ. 245, 118014. https://doi.org/10.1016/j.atmosenv.2020.118014.

Liu, Z., Wang, Y., Vrekoussis, M., Richter, A., Wittrock, F., Burrows, J.P., Shao, M., Chang, C.C., Liu, S.C., Wang, H., Chen, C., 2012. Exploring the missing source of glyoxal (CHOCHO) over China. Geophys. Res. Lett. 39, L10812. https://doi.org/10.1029/2012gl051645.

McCarthy, M.C., Aklilu, Y.-A., Brown, S.G., Lyder, D.A., 2013. Source apportionment of volatile organic compounds measured in Edmonton, Alberta. Atmos. Environ. 81, 504–516. https://doi.org/10.1016/j.atmosenv.2013.09.016.

MEP (Ministry of Ecology and Environment of the People's Republic of China), 2014. Guidebooks for compiling air pollution emission inventories. Available at: http://www.zhb.gov.cn/gkml/hbb/bgg/201408/t20140828_288364.htm.

MEP (Ministry of Ecology and Environment of the People's Republic of China), 2015a. Ambient air- determination of volatile organic compounds- collected by specially-prepared canisters and analyzed by gas chromatography/mass spectrometry (HJ759-2015). Available at: http://www.mee.gov.cn/ywgz/fgbz/bz/bzwb/jcffbz/201510/W020151030573530793420.pdf.

MEP (Ministry of Ecology and Environment of the People's Republic of China), 2015b. Guidelines for NMVOCs pollution source investigation in petrochemical industry. Available at: http://www.mee.gov.cn/gkml/hbb/bgt/201511/W020151124546327744099.pdf.

NJNBS (Nanjing Bureau of Statistics), 2018. Statistical Yearbook of Nanjing. China Statistics Press in Chinese.

Mo, Z., Shao, M., Lu, S., 2016. Compilation of a source profile database for hydrocarbon and OVOC emissions in China. Atmos. Environ. 143, 209–217. https://doi.org/10.1016/j.atmosenv.2016.08.025.

Mochizuki, T., Miyazaki, Y., Ono, K., Wada, R., Takahashi, Y., Saigusa, N., Kawamura, K., Tani, A., 2015. Emissions of biogenic volatile organic compounds and subsequent formation of secondary organic aerosols in a Larix kaempferi forest. Atmos. Chem. Phys. 15, 12029–12041. https://doi.org/10.5194/acp-15-12029-2015.

Ou, J., Zheng, J., Li, R., Huang, X., Zhong, Z., Zhong, L., Lin, H., 2015. Speciated OVOC and VOC emission inventories and their implications for reactivity-based ozone control strategy in the Pearl River Delta region, China. Sci. Total Environ. 530–531, 393–402. https://doi.org/10.1016/j.scitotenv.2015.05.062.

Qiao, X., Wang, P., Zhang, J., Zhang, H., Tang, Y., Hu, J., Ying, Q., 2019. Spatial-temporal variations and source contributions to forest ozone exposure in China. Sci. Total Environ. 674, 189–199. https://doi.org/10.1016/j.scitotenv.2019.04.106.

Skamarock, W.C., Klemp, J.B., Dudhia, J., Gill, D.O., Barker, D.M., Duda, M.G., Huang, X.-Y., Wang, W., Powers, J.G., 2008. A Description of the Advanced Research WRF Version 3. NCAR Technical Note. https://doi.org/10.5065/D68S4MVH 2008.

Shao, M., Huang, D., Gu, D., Lu, S., Chang, C., Wang, J., 2011. Estimate of anthropogenic halocarbon emission based on measured ratio relative to CO in the Pearl River Delta region, China. Atmos. Chem. Phys. 11, 5011–5025. https://doi.org/10.5194/acp-11-5011-2011.

Simayi, M., Shi, Y., Xi, Z., Li, J., Yu, X., Liu, H., Tan, Q., Song, D., Zeng, L., Lu, S., Xie, S., 2020. Understanding the sources and spatiotemporal characteristics of VOCs in the Chengdu plain, China, through measurement and emission inventory. Sci. Total Environ. 714, 136692. https://doi.org/10.1016/j.scitotenv.2020.136692.

SMBEE (Shanghai Municipal Bureau of Ecology and Environment), 2017. Estimation methods of volatile organic compounds emissions from industrial plants in Shanghai. Available at: https://sthj.sh.gov.cn/hbzhywpt1133/hbzhywpt1135/20170308/0024-103293.html.

Thera, B.T.P., Dominutti, P., Öztürk, F., Salameh, T., Sauvage, S., Afif, C., Çetin, B., Gaimoz, C., Keleş, M., Evan, S., Borbon, A., 2019. Composition and variability of gaseous organic pollution in the port megacity of Istanbul: source attribution, emission ratios, and inventory evaluation. Atmos. Chem. Phys. 19, 15131–15156. https://doi.org/10.5194/acp-19-15131-2019.

Toro, M.V., Cremades, L.V., Calbó, J., 2006. Relationship between VOC and NOx emissions and chemical production of tropospheric ozone in the Aburrá Valley (Colombia). Chemosphere 65, 881–888. https://doi.org/10.1016/j.chemosphere.2006.03.013.

USEPA (U.S. Environmental Protection Agency), 2014. SPECIATE Version 4.4. Available at: https://www3.epa.gov/ttnchie1/software/speciate.

Wang, M., Shao, M., Chen, W., Yuan, B., Lu, S., Zhang, Q., Zeng, L., Wang, Q., 2014. A temporally and spatially resolved validation of emission inventories by measurements of ambient volatile organic compounds in Beijing, China. Atmos. Chem. Phys. 14, 5871–5891. https://doi.org/10.5194/acp-14-5871-2014.

Wang, H., Yan, R., Xu, T., Wang, Y., Wang, Q., Zhang, T., An, J., Huang, C., Gao, Y., Gao, Y., Li, X., Yu, C., Jing, S., Qiao, L., Lou, S., Tao, S., Li, Y., 2020a. Observation constrained aromatic emissions in Shanghai, China. J. Geophys. Res. Atmos. 125. https://doi.org/10.1029/2019jd031815.

Wang, M., Chen, W., Zhang, L., Qin, W., Zhang, Y., Zhang, X., Xie, X., 2020b. Ozone pollution characteristics and sensitivity analysis using an observation-based model in Nanjing, Yangtze River Delta region of China. J. Environ. Sci. 93, 13–22. https://doi.org/10.1016/j.jes.2020.02.027.

Warneke, C., McKeen, S., De Gouw, J., Goldan, P., Kuster, W., Holloway, J., Williams, E., Lerner, B., Parrish, D., Trainer, M., 2007. Determination of urban volatile organic compound emission ratios and comparison with an emissions database. J. Geophys, Res, Atmos. 112, D10S47. https://doi.org/10.1029/2006JD007930.

Wu, R., Zhao, Y., Zhang, J., Zhang, L., 2020. Variability and sources of ambient volatile organic compounds based on online measurements in a suburban region of Nanjing, Eastern China. Aerosol Air Qual. Res. https://doi.org/10.4209/aaqr.2019.10.0517.

Wu, R.R., Xie, S.D., 2017. Spatial distribution of ozone formation in China derived from emissions of speciated volatile organic compounds. Environ. Sci. Technol. 51, 2574–2583. https://doi.org/10.1021/acs.est.6b03634.

Yáñez-Serrano, A.M., Nölscher, A.C., Bourtsoukidis, E., Derstroff, B., Zannoni, N., Gros, V., Lanza, M., Brito, J., Noe, S.M., House, E., Hewitt, C.N., Langford, B., Nemitz, E., Behrendt, T., Williams, J., Artaxo, P., Andreae, M.O., Kesselmeier, J., 2016. Atmospheric mixing ratios of methyl ethyl ketone (2-butanone) in tropical, boreal, temperate and marine environments. Atmos. Chem. Phys. 16, 10965–10984. https://doi.org/10.5194/acp-16-10965-2016.

Yang et al., in preparation Yang, J., Zhao, Y., Zhang, L., in preparation. Performance and application of chemical transport models on ozone simulation in China – a review.

Yang, Y., Zhao, Y., Zhang, L., Zhang, J., Huang, X., Zhao, X., Zhang, Y., Xi, M., Lu, Y., 2021. Improvement of the satellite-derived NOx emissions on air quality modeling and its effect on ozone and secondary inorganic aerosol formation in the Yangtze River Delta, China. Atmos. Chem. Phys. 21, 1191–1209. https://doi.org/10.5194/acp-21-1191-2021.

Yuan, X.Y., Xu, Y., Du, Y.D., Feng, Z.Z., 2021. Differences of biogenic volatile organic compound (BVOC) emissions from urban forests in Nanjing and Beijing. (in Chinese) https://doi.org/10.19674/j.cnki.issn1000-6923.20211025.002 (in Chinese).

Zhang, L., Zhu, X., Wang, Z., Zhang, J., Liu, X., Zhao, Y., 2021. Improved speciation profiles and estimation methodology for VOCs emissions: a case study in two chemical plants in eastern China. Environ. Pollut. 291, 118192. https://doi.org/10.1016/j.envpol.2021.118192.

Zhao, Q., Bi, J., Liu, Q., Ling, Z., Shen, G., Chen, F., Qiao, Y., Li, C., Ma, Z., 2020. Sources of volatile organic compounds and policy implications for regional ozone pollution control in an urban location of Nanjing East, China. Atmos. Chem. Phys. 20, 3905–3919. https://doi.org/10.5194/acp-20-3905-2020.

Zhao, Y., Huang, Y.W., Xie, F.J., Huang, X., Yang, Y., 2021. The effect of recent controls on emissions and aerosol pollution at city scale: A case study for Nanjing, China. Atmos. Environ. 246, 118080. https://doi.org/10.1016/j.atmosenv.2020.118080.

Zhao, Y., Mao, P., Zhou, Y., Yang, Y., Zhang, J., Wang, S., Dong, Y., Xie, F., Yu, Y., Li, W., 2017. Improved provincial emission inventory and speciation profiles of anthropogenic non-methane volatile organic compounds: a case study for Jiangsu, China. Atmos. Chem. Phys. 17, 7733–7756. https://doi.org/10.5194/acp-17-7733-2017.

Zhao, Y.H., Zhang, L., Zhou, M., Chen, D., Lu, X., Tao, W., Liu, J.F., Tian, H., Ma, Y.P., Fu, T.M., 2019. Influences of planetary boundary layer mixing parameterization on summertime surface ozone concentration and dry deposition over North China. Atmos. Environ. 218, 116950. https://doi.org/10.1016/j.atmosenv.2019.116950.

Zheng, H., Kong, S., Xing, X., Mao, Y., Hu, T., Ding, Y., Li, G., Liu, D., Li, S., Qi, S., 2018. Monitoring of volatile organic compounds (VOCs) from an oil and gas station in Northwest China for 1 year. Atmos. Chem. Phys. 18, 4567–4595. https://doi.org/10.5194/acp-18-4567-2018.

Zhong, Z., Zheng, J., Zhu, M., Huang, Z., Zhang, Z., Jia, G., Wang, X., Bian, Y., Wang, Y., Li, N., 2018. Recent developments of anthropogenic air pollutant emission inventories in Guangdong province, China. Sci. Total Environ. 627, 1080–1092. https://doi.org/10.1016/j.scitotenv.2018.01.268.

Zhou, Y., Zhao, Y., Mao, P., Zhang, Q., Zhang, J., Qiu, L., Yang, Y., 2017. Development of a high-resolution emission inventory and its evaluation and application through air quality modeling for Jiangsu Province, China. Atmos. Chem. Phys. 17, 211–233. https://doi.org/10.5194/acp-17-211-2017.